Effect of the Degree of Clay Delamination on the Phase Morphology, Surface Chemical Aspects, and Properties of Hydrolyzable Polyurethanes for Periodontal Regeneration

I. M. Pereira,[1] S. Carvalho,[2] M. M. Pereira,[2] M. F. Leite,[3] R. L. Oréfice[2]

[1]*Department of Metallurgy, Federal Center of Technological Education of Minas Gerais, Timoteo, Brazil*
[2]*Department of Metallurgical and Materials Engineering, Federal University of Minas Gerais, Belo Horizonte, Brazil*
[3]*Department of Physiology and Biophysics, ICB/UFMG, Federal University of Minas Gerais, Minas Gerais, Brazil*

Received 27 November 2008; accepted 13 March 2009
DOI 10.1002/app.30404
Published online 2 June 2009 in Wiley InterScience (www.interscience.wiley.com).

ABSTRACT: In recent years, there has been increased interest in biodegradable polyurethanes for use in regenerative medicine because of their versatility and biocompatibility. Nevertheless, these polymers are usually produced using organic solvents that can lead to the release of toxic components. In this work, polyurethane/montmorillonite nanocomposites were designed to work as guided tissue regeneration membranes to treat periodontal diseases. Polyurethanes were synthesized in an aqueous environment. The composition, morphology, and mechanical properties of the biomaterials were evaluated. The cellular viability, proliferation, and morphology changes of rat culture cementoblasts were also investigated using a montmorillonite assay. Small-angle X-ray scattering, X-ray diffraction, and infrared spectroscopy results showed that the degree of clay delamination within the polymer was able to tailor the phase morphology of the polymer, the chemical aspects of the surface, the mechanical properties, and the kinetics of hydrolysis of the materials. The produced scaffolds provided a good environment for the adhesion and proliferation of cementoblasts and thus can be considered suitable biomaterials for participating in procedures associated with periodontal regeneration. © 2009 Wiley Periodicals, Inc. J Appl Polym Sci 114: 254–263, 2009

Key words: polyurethane; montmorillonite; tissue regeneration

INTRODUCTION

A family of polymers that contains urethane linkages is very often called polyurethanes (PUs). PUs can be designed and produced to yield thermoplastic elastomers that have segmented macromolecular architecture formed by hard (polar) and soft (nonpolar) segments. The properties of this type of material will, therefore, be strongly associated with the hard and soft segments: content, interaction, and phase separation.[1,2] Recently, polyurethane/montmorillonite nanocomposites (PU/MMT) have been studied to produce materials with improved properties that could extend the use of PU further.[3] To achieve high levels of properties in polymer nanocomposites, the dispersion and exfoliation of layered silicates within polymeric matrices are considered key steps. Since natural montmorillonite has poor affinity with hydrophobic polymers, cationic modified MMT has been widely used[3,4] to improve interfacial interactions and exfoliation.

Segmented PUs have been extensively used in biomedical applications because of their biocompatibility; typical examples are catheters, skin wound dressings, tissue adhesives, etc.[5] Therefore, there has been increased interest in biodegradable PUs for use as tissue scaffolds and drug delivery systems. Designed to undergo hydrolytic or enzymatic degradation, the tissue-engineered scaffolds are intended to be used in regenerative medicine, for instance, regeneration of cardiovascular, musculoskeletal, and neurological tissues.[6] However, these PUs are usually produced using organic solvents that can lead potentially to the release of carcinogenic components.[7] As a consequence, PUs synthesized in an aqueous environment (waterborne PUs) can be very useful in reducing the risk of toxic components derived from organic solvents.

In recent years, tissue engineering strategies were associated with the concepts of guided tissue regeneration (GTR) to promote periodontal wound healing. GTR was first introduced in 1982 by Nyman et al.[8] Nowadays, it has become an essential part of clinical periodontics[9,10] to treat periodontal disease, which is characterized by inflammation and subsequent loss or damage of tooth-supporting tissues,

Correspondence to: R. L. Oréfice (rorefice@demet.ufmg.br).
Contract grant sponsors: National Council for Scientific and Technological Development (CNPq), The State of Minas Gerais Research Foundation (FAPEMIG).

including cementum, bone, and periodontal ligament. The GTR clinical method involves exclusion of epithelium and isolation of the root surface from gingival corium by a physical barrier in the form of a membrane. These barriers act as filters to prevent epithelial and connective tissue cell migration to facilitate regenerative potential cells to proliferate and migrate into the protected wound area.[10] A variety of synthetic and naturally derived GTR membranes have been used to facilitate periodontal tissue regeneration. Gore-Tex and TefGen belong to the first generation of GTR membranes, which are characterized by being nonabsorbable.[8] Barrier membranes must meet certain requirements, such as (i) tissue integration to promote wound stabilization; (ii) cell occlusivity to attract desirable cells such as periodontal ligament cells, bone cells, and cementoblasts, (iii) space-making and/or maintaining to allow new attachment formation, and (iv) biocompatibility to ensure material safety.[9] However, other factors such as adequate mechanical properties and biodegradation contribute to tissue regeneration. The mechanically dynamic environment in the mouth requires a material capable to resist tribological movements occurring in the mouth and a material able to sustain and recover form after various deformations without irritation to the surrounding tissues. Moreover, the use of a biodegradable membrane would eliminate the necessity of a second surgical procedure for the removal of the membrane and may thereby facilitate the clinical use of the GTR strategy. For that reason, a second generation of absorbable GTR membrane has rapidly gained interest.[8]

The aim of the present study was to develop a soft, tough, and elastomeric PU with potential application as GTR membrane. In this work, PUs were synthesized in an aqueous environment by combining hard segments derived from aliphatic isophorone diisocyanate and hydrazine with soft segments based on poly(caprolactone diol). PUs were also reinforced with Na^+/MMT. The composition, morphology, and mechanical properties of the biomaterials were investigated. Cementoblasts were used in this study to evaluate the cellular response to PU/MMT membranes. Cementoblasts are cells adjacent to the dentine responsible for the cementogenesis. Cementogenesis is the creation of cementum, a hard mineralized tissue, which covers the roots of teeth and provides attachment of periodontal ligament to roots and surrounding alveolar bone. Cementum is essential for periodontal regeneration, as it provides anchorage between the root surface and periodontal ligament.[11–17] Therefore, biodegradable biomaterials that can support the growth of cementoblasts are potential strong candidates to be used in periodontal regeneration.

MATERIALS AND METHODS

Polymer synthesis

Poly(caprolactone diol) (PCL $M_n = 1250$ g/mol), isophorone diisocyanate (IPDI), 2,2-bis(hydroxymethyl) propionic acid (DMPA), and dibutyl tin dilaurate (DBDLT) were obtained from Aldrich (St. Louis, MO). Triethylamine (TEA, 98%) and hydrazine (HZ, 25%) were purchased from Vetec (RJ, Brazil). All these chemicals were used throughout this work without any previous treatment. Natural MMT (Cloisite® Na^+) was obtained from Southern Clay (Gonzales, TX).

PUs were synthesized by the conventional prepolymer method, using a 250-mL, three-necked glass flask equipped with a heating mantel, a mechanical stirrer, and a thermometer under nitrogen atmosphere. In the first step, prepolymer was obtained by reacting PCL (20.12 wt %), DMPA (1.63 wt %), and IPDI (12.55 wt %) at 2 NCO/OH ratio for approximately 3.5 h. During this time, DBDLT was added twice. The reaction was carried out at 70–75°C. After cooling down to 40°C, the carboxylic acid groups were neutralized by the addition of TEA (1.23 wt %). The mixture was then gently stirred for 40 min. The dispersion in water and PU chain extension were achieved by adding HZ (0.77 wt %) and deionized water (63.70 wt %) to the neutralized prepolymer under high-speed stirring. To ensure that the reaction was completed, the mixture was stirred for 60 min. This chemical procedure was well succeeded in producing PU water dispersions with solid content of approximately 30%. The weight fraction (%) of hard segment, W (HS), is 38% (IPDI + HZ).

Nanocomposites

PU/MMT nanocomposites were prepared via solution blending. Initially, the MMT water dispersion was produced by mixing the clay (5 wt %) with deionized water for 24 h at 65°C. The PU water dispersion was blended with the MMT water dispersion at room temperature under mechanical stirring for 15 min. The samples with different MMT weight contents were numbered as PU/MMT-1, PU/MMT-2, PU/MMT-3, PU/MMT-4, and PU/MMT-5, corresponding to MMT weight contents of 0%, 0.4%, 1.2%, 2.0%, and 4.0%, respectively.

Films were produced by casting the dispersions in a PVC mold and allowing them to dry at 17°C for 1 week. The films were then annealed at 80°C for 72 h.

Characterization

Infrared spectra were collected in a Fourier transform infrared spectrophotometer (FTIR; Perkin–Elmer, model Spectrum 1000). Measurements were

carried out using the attenuated total reflectance (ATR) technique. Each spectrum was a result of 64 scans with a resolution of 4 cm^{-1}.

Wide angle X-ray scattering (WAXS) analysis was performed in thin samples having thicknesses ranging from 0.8 to 1.0 mm and 15 mm in diameter, using a Philips model PW1710 diffractometer operated with Cu Kα irradiation at a scan rate of 2° 2θ/s in the range of 3°–60°.

Small angle X-ray scattering (SAXS) measurements of synchrotron small angle X-ray scattering were performed using the beam line of the National Synchrotron Light Laboratory (LNLS, Campinas, Brazil). After passing through a thin beryllium window, the beam is monochromatized (λ = 1.488 Å) and horizontally focused by a cylindrically bent and asymmetrically cut silicon single crystal. The X-ray scattering intensity, $I_{(q)}$, was experimentally determined as a function of the scattering vector, q, whose modulus is given by eq. (1):

$$q = \frac{4\pi}{\lambda}\sin\theta \tag{1}$$

where λ is the X-ray wave length and θ is half of the scattering angle. Each SAXS pattern corresponds to a data collection time of 900 s.

Static mechanical tests were performed using a universal testing machine (DL3000, EMIC) at 10 mm/min crosshead speed (DIN60). Samples were deformed up to 500% deformation. The tensile strength (σ_m), initial modulus (E), and toughness of the samples were extracted from the curves. The sample length between the clamps was 20 mm. The tests were performed at 28°C (room temperature).

Swelling of PU/MMTs was carried out in deionized water at 37°C using films 15 mm in diameter. The sample mass-to-water volume ratio was kept constant and equal to 1/50 g/cm^3. The samples were removed from water at the preselected time intervals, wiped gently, and weighed using an analytical balance. Changes in sample weight were calculated according to eq. (2):

$$\text{Water uptake}\,(\%) = \frac{w_t - w_0}{w_0} \times 100 \tag{2}$$

where w_0 and w_t were the initial weight and the weight at time t, respectively. The average of three measurements was used to plot the results.

Preliminary information regarding the biodegradation of the materials was obtained by submitting them to hydrolysis at high pH. This type of biodegradation test was performed by weighing samples 10 mm in diameter and immersing them in an NaOH 3 wt % aqueous solution. The samples were removed from the media at preselected time intervals, rinsed three times with distilled water, and immersed in distilled water for another hour. The specimens were then dried to a constant weight at 37°C for 1 week and weighed using an analytical balance to determine the weight loss. The average of three measurements was used to report the results. The weight loss of the polymer films after degradation was evaluated as the residual weight (%), which was defined by eq. (3):

$$\text{Residual weight}\,(\%) = 100 - \left(\frac{w_0 - w_t}{w_0} \times 100\right) \tag{3}$$

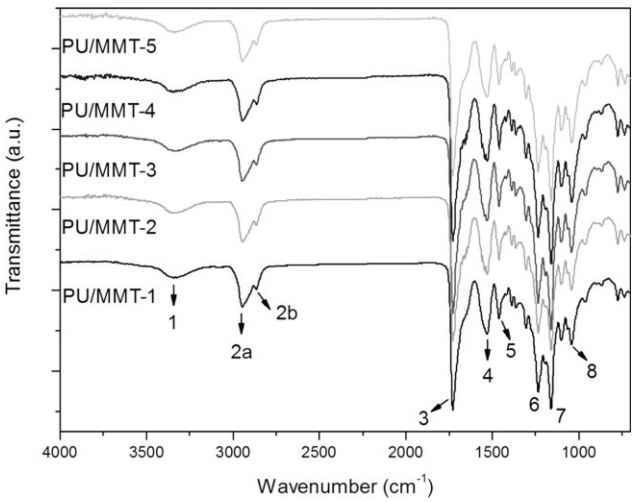

Figure 1 FTIR spectra of PU/MMT-1 to PU/MMT-5 samples.

Cell culture and viability assays

Extraction and direct contact tests were used to evaluate the cytotoxicity of the PU nanocomposites. Cementoblasts were isolated from the molars extracted from Wistar male rats (8 weeks old, 220–250 g).[18] The extracted molars were rinsed with Dulbecco's phosphate-buffered saline solution without calcium and magnesium. The molars were then immersed in a digestion solution, produced with the following components: 20 mL of Dulbecco's modified Eagle medium (DMEM) containing 0.04 collagenase (180 U/mL) and 0.5 mL trypsin at 37°C. This solution was used for five consecutive digestions, and five cell populations were obtained at the end. The first two populations were discarded, whereas the other three produced a suspension of periodontal ligament cells that includes cementoblasts. The three suspensions of cells were centrifuged for 5 min at 1000 g. The cells of each population were then cultured in DMEM with 10% fetal bovine serum, penicillin G (10 U/mL), streptomycin sulfate (10 mg/mL), and 0.25 anfotericin-b in a humidified atmosphere of 5% CO_2 at 37°C. The cells were used for experiments at passage two. Cementoblasts cells were identified by RT-PCR and Western blot F-spondin cell marker.

TABLE I
Relationship between FTIR Absorption Bands and Functional Group Observed in Figure 1

Bands	Origin	Frequency (cm^{-1})	Assignment
1	N—H	3,600–3,150	Primary amine stretching vibration mode
		~3,500	Free N—H stretching vibration band
		~3,300	Hydrogen bonded N—H vibration band
2	—CH_3	3,000–2,800	Methylene stretching vibration modes
3	C=O	1,760–1,600	Carbonyl groups stretching vibrations
		1,750–1,725	Ester stretching vibration modes
		~1,720	Free urethane stretching vibration band
		~1,700	Hydrogen bonded urethane stretching vibration band
		~1,660	Free urea stretching vibration band
		~1,630	Hydrogen bonded urea stretching vibration band
4	>N—H	1,640–1,540	Secondary amide vibration modes
5	—CH_3	1,470–1,430	Methylene groups asymmetric bend vibration modes
6	C—N	1,292–1,226	Tertiary amide stretching vibration modes
7	C—O—C	1,150	Ether stretching vibration
8	Si—O	1,038	Stretching vibration mode

Cementoblasts were plated in 24-well plates, and, after 2 h, their viability was evaluated by using the MTT assay. This assay quantifies cell viability based on the reduction of tetrazolium salt to formazan crystals.[16] The PU/MMT samples were sterilized by UV radiation. Three samples were used in each MTT assay. In this study, cells were cultured on wells without PU samples to be used as positive controls and wells with no cells (only medium) were used as the negative control. Cementoblasts were seeded in contact with PU/MMT samples at density of 1×10^5 cells/cm and then incubated at 37°C and 5% CO_2. After 2 h of incubation, the cells on the materials were observed by optical microscopy. After 72 h of incubation, the culture medium was adjusted to 210 μL, and 170 μL of MTT (5 mg/mL) was added to each well. Four hours later, formazan salts were dissolved with isopropanol. Then, 100 μL of the solution from each well was aspirated and poured into a 96-well plate for absorbance measurement at 595 nm.[16] The absorbance was directly proportional to cell viability. Results are expressed as percentage of cell viability.

Data were statically analyzed by using the GraphPad Prism signed rank test. The results, expressed as the average of triplicate wells, were repeated three times. A total of nine wells were assayed in each experimental group. Probabilities less than 0.05 were considered as significant.

RESULTS AND DISCUSSION

Infrared spectroscopy

Typical infrared spectra of PU/MMT-1, PU/MMT-2, PU/MMT-3, PU/MMT-4, and PU/MMT-5 are shown in Figure 1. The characteristic absorption bands of poly(ester-urethanes) are assigned in Figure 1 and described in Table I, where each absorption band frequency and the correspondent functional

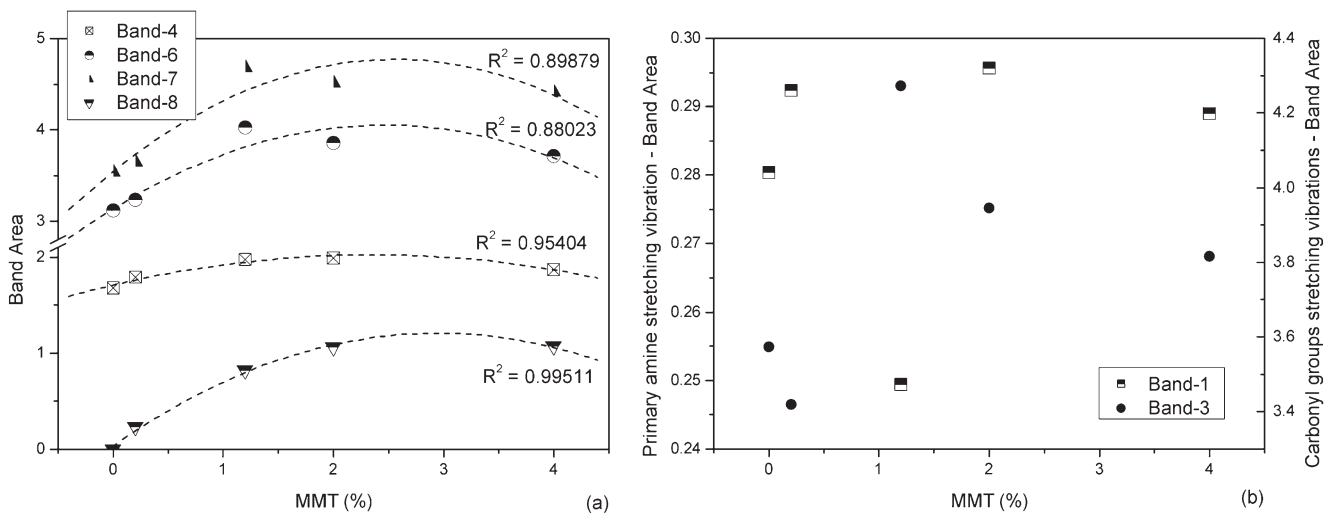

Figure 2 Influence of filler content on band area of PU/MMT-1 to PU/MMT-5: (a) bands 4 and 6 to 8, (b) bands 1 and 3.

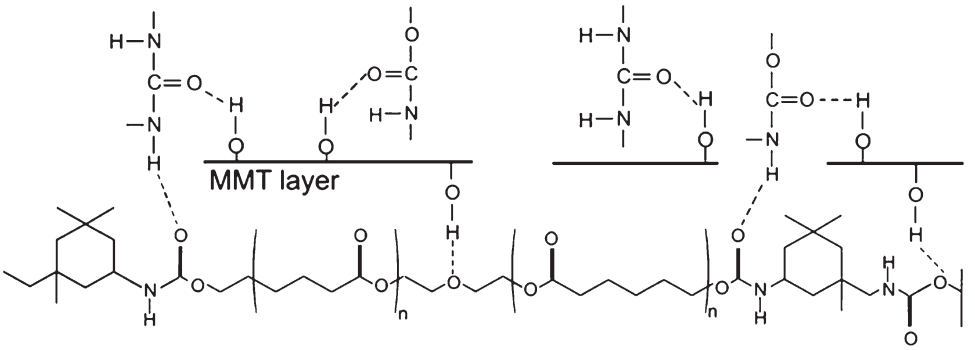

Figure 3 Hydrogen bonding interaction between PU and MMT layer.

group are reported. To compensate for differences in signal intensity, the infrared spectra were normalized according to the —CH_3 region (3000–2800 cm^{-1}). It was observed that the position of the absorption bands of each specific functional group listed in Table I was similar both for PU/MMT-1 and PU/MMT-2 to PU/MMT-5 composites.[19–28]

To obtain more detailed information regarding bands 1, 3, 4, and 6 to 8, the area under each band was calculated using the Origin® software. It is possible to draw a second order polynomial regression for curves where the area of bands 4 and 6 to 8 is plot as a function of the amount of MMT in PUs. The obtained curves show a good 2nd-order correlation factor [Fig. 2(a)]. Because the FTIR-ATR technique provides only surface information, up to 3 μm, the 2nd-order behavior may indicate that the presence of the filler modifies chain mobility and phase structure, allowing the migration of polar groups to the surface in samples having MMT up to 2%. For higher concentrations of MMT, clay reagglomeration may occur, and the resulting tactoids will be less effective in disturbing chain dynamics and phase morphology. However, no direct correlation between band areas of bands 1 and 3 [Fig. 2(b)] and the composition of the systems could be drawn, indicating that a series of factors may affect these chemical functionalities when exposed to clay nanoparticles.

Bands 1 and 3 are usually related to the hydrogen bonding in segmented PU. In recent years, the relationship between specific interactions of bands 1 and 3 and the phase behavior of polymer nanocomposites has been proposed.[27] In Figure 3,[27] possibilities of hydrogen bonding between MMT and PU matrix are sketched. The hydrogen bonding interactions occur between the hydroxyl group of MMT (proton donor) with proton–acceptor entity of PUs such as urea, urethane, and ether.[27,29] Because the absorption band 1 overlaps band 3, a deconvolution mathematical procedure (by using the PickFiT® software) was performed on spectra of Figure 1 to enhance resolution of each individual band. Figure 4(a,b) illustrates, respectively, the deconvolution of the N—H region and the deconvolution of the carbonyl stretching region of PU/MMT samples.

The ratio between the absorption band areas of bonded and free NH represents the NH groups, which are hydrogen bonded. The extent of the carbonyl groups participating in hydrogen bonding in

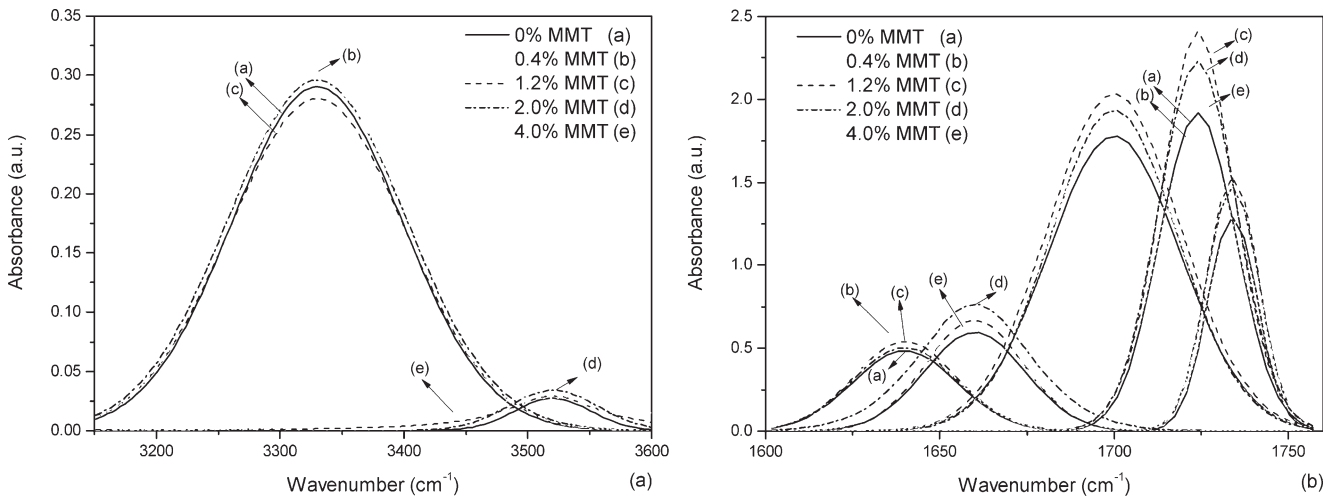

Figure 4 Deconvoluted FTIR spectrum: (a) N—H stretching region, (b) carbonyl stretching region.

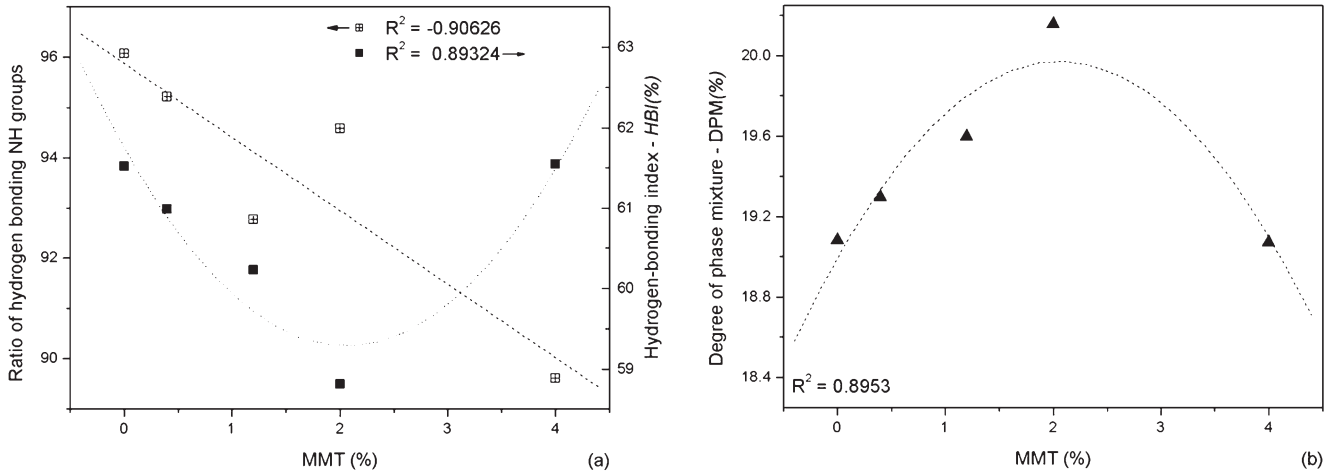

Figure 5 Influence of filler content on: (a) ratio of hydrogen bonding NH groups and HBI (%) and (b) phase mixture.

PUs can be expressed by a hydrogen-bonding index HBI (%), which is described by eq. (4)[2,27]:

$$\text{HBI } (\%) = \frac{A_{1700}}{(A_{1700} + A_{1720})} \times 100 \tag{4}$$

where A_{1700} and A_{1720} are, respectively, the FTIR absorption band area of free urethane at 1720 cm^{-1} and bonded urethane at 1700 cm^{-1}.

Figure 5(a) shows that the ratio between hydrogen-bonded NH groups and free NH groups is slightly dependent on the MMT content. It can be seen that the NH bands of MMT/PUs are all nearly completely hydrogen bonded. Figure 5(a) shows the 2nd-order relationship between *HBI* (%) and MMT (%); the plot suggests that the amount of carbonyl groups participating in hydrogen bonding in PU/MMTs goes through a minimum at clay contents close to 2 wt %. Well-dispersed nanoparticles derived from clay can disturb the formation of hard and soft domains by reducing the mobility of the chain segments confined at the clay surfaces and by restricting the formation of hydrogen bonds between amine and carbonyl groups. These facts can lead to materials having an enhanced degree of phase mixing. The introduction of clay nanoparticles into PU in concentrations higher than 2 wt % can lead to the production of agglomerates (tactoids) during film formation. The presence of agglomerates can reduce interfacial area and interactions between the polymer and clay particles. The degree of phase mixture, *DPM* (%), can be calculated from FTIR data as expressed eq. (5).[29] Results are summarized in Figure 5(b).

$$\text{DPM } (\%) = \frac{(1 - \text{HBI } (\%)) \times \text{W(HS)}}{(1 - \text{HBI } (\%)) \times \text{W(HS)} + (1 - \text{W(HS)})} \tag{5}$$

Clay agglomerates are much larger than PU domains, and phase separation would not be highly affected when agglomerates, instead of high aspect ratio nanoparticles, are present. Therefore, FTIR data suggest that the incorporation of clay particles up to 2 wt % MMT can result in highly well-dispersed and delaminated clay platelets, whereas PUs containing clay particles in concentrations higher than 2 wt % MMT can lead to particle reagglomeration during film formation.

Wide-angle X-ray scattering

Two types of polymer-layered nanocomposites are well described in the literature: intercalated nanocomposites and exfoliated nanocomposites. In the former, the polymer chains alternate with the inorganic layers in a fixed compositional ratio to yield a well-defined number of polymer layers in the intralamellar space. In this case, the WAXS patterns of intercalated nanocomposites show usually diffraction peaks associated with the interlayer distance at lower diffraction angles (2θ between 3° and 10°). In

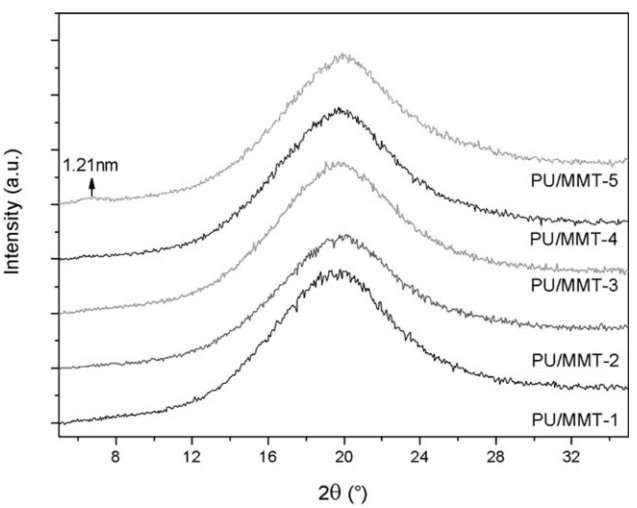

Figure 6 WAXS pattern of PU/MMT-1 to PU/MMT-5.

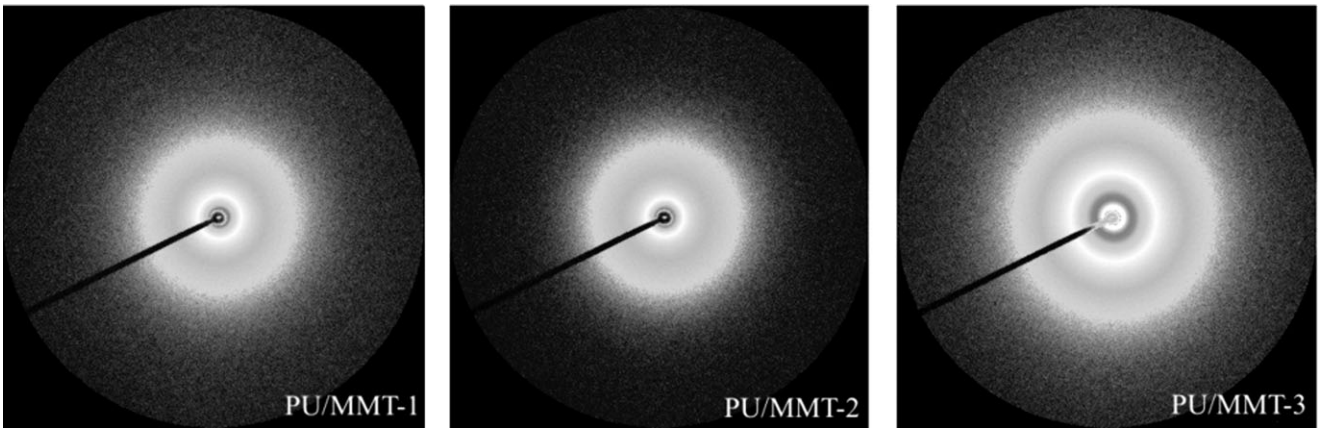

Figure 7 SAXS pattern of: (a) PU/MMT-1, (b) PU/MMT-2, and (c) PU/MMT-3.

exfoliated nanocomposites, no diffraction peaks are shown, the number of polymer chains between the layers is almost continuously variable, and the layers stand >10 nm apart.[30–32] Figure 6 shows the WAXS patters of PUs nanocomposites containing different amounts of MMT.

No major diffraction peaks were observed for PU/MMTs, which can be related to the amorphous nature of poly(ester-urethane) produced by using low molar mass PCL diols ($M_n < 2000$ g/mol) and low soft segment contents. Poly(ester-urethane) containing soft segments based on low molar mass PCL can present low degrees of phase separation that restrict soft segment segregation and therefore crystallization.[33] The large halo around $2\theta = 20^\circ$ on the WAXS curves is typical of materials that have only short-range order.[33–36]

Previous studies[32] showed that the diffraction peak of the MMT/Na^+ occurs around $2\theta = 7.4^\circ$, corresponding to the interlayer spacing of 1.21 nm. Thus, the disappearance of peaks around $2\theta = 2^\circ$–10° may indicate that the silicate layers were completely exfoliated and distributed uniformly within the amorphous domains in the PU matrix, being a nanometer-scaled composite. However, in PU/MMT-5, a small and broad diffraction peak around $2\theta = 7.4^\circ$ can be observed, which implies that part of the clay had reagglomerated during the drying stage.

Small-angle X-ray scattering

Figure 7(a–c) shows, respectively, SAXS patterns of PU/MMT-1, PU/MMT-2, and PU/MMT-3. PU/MMT-4, and PU/MMT-5 SAXS experiments were not carried out. As expected from the randomly distributed particles embedded in an amorphous matrix, a circular scattering pattern with a homogeneous intensity distribution along the circle was obtained. The symmetric scattering patterns of PU/MMTs indicate that the films are isotropic.

SAXS profiles as a function of the scattering vector, q, are shown in Figure 8(a). SAXS profiles do not exhibit any peak, confirming WAXS results and indicating that a high degree of exfoliation can be achieved by the clay dispersion, during mixing with PUs water dispersion. Further evaluation was obtained by applying the Lorentz correction on SAXS data [Fig. 8(b)]. The Lorentz correction describes the electron density fluctuation

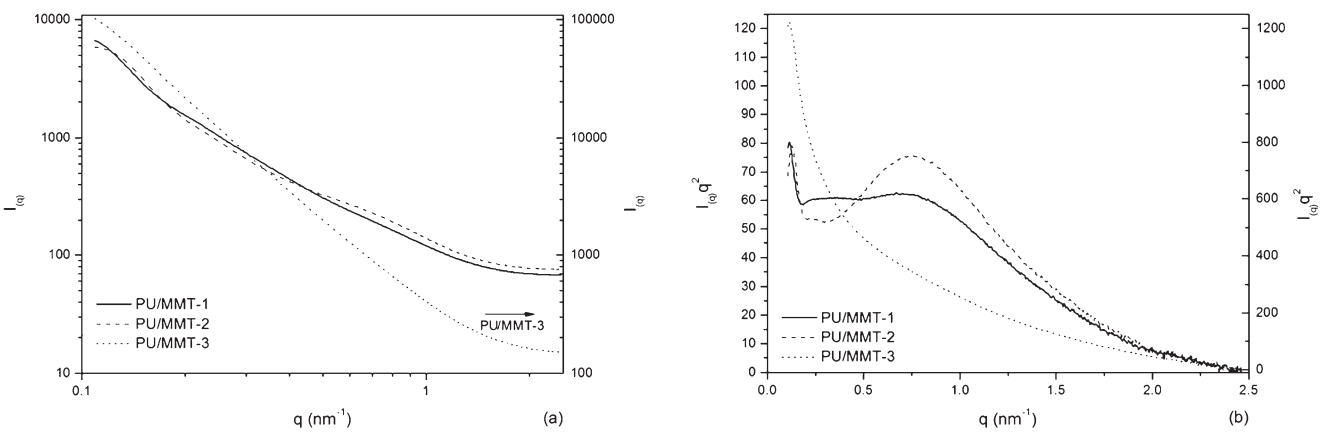

Figure 8 (a) SAXS profiles of PU/MMT-1, PU/MMT-2, and PU/MMT-3, and (b) Lorentz correction.

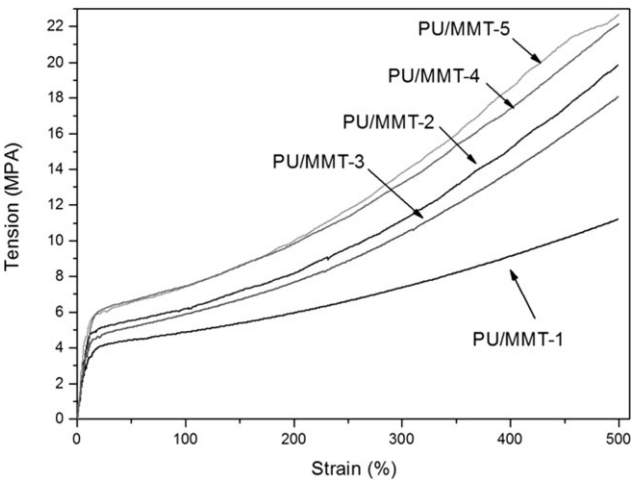

Figure 9 Stress–strain curves of PU/MMT-1 to PU/MMT-5.

of polymer and is a good description of overall phase separation.

The PU/MMT-1–corrected profile displays a broad scattering peak around $q = 0.78$ nm^{-1}. This peak characterizes the presence of domains having different electronic densities that can be associated with the phase separation derived from the incompatibility between soft and hard segments in PU. Scattering data in Figure 8 also show that the presence of clay nanoparticles disturbed the phase separation of the system, changing the matrix morphology. At low filler content, the scattering peak due to the PU phase separation became narrowed, attesting the gradual increase of the hard–soft-segment degree of mixing. It is also possible to observe that scattering increased due to the presence of clay particles. Having clay particles with higher electronic density than PU matrix, the scattered radiation achieves higher levels when nanoparticles were incorporated into PU. The same phenomenon is observed at the PU/MMT-3 SAXS profile, which is 10 times more intense due to the presence of 1.2 wt % MMT. At 1.2 wt % MMT composition, no scattering peak can be observed, demonstrating that a high degree of phase mixture was obtained. The SAXS results agree with WAXS and DPM (%) results described previously, confirming that a high degree of exfoliation can be achieved by the clay dispersion during mixing with PU water dispersion for compositions with low clay content (<1.2 wt % MMT).

Mechanical properties

Figure 9 shows typical stress–strain curves for PU/MMT samples. Table II summarizes the values for the mechanical properties. The values of toughness and resilience in Table II were obtained by integrating the stress–strain curves, and they can represent, respectively, the energy absorbed up to 500% deformation and the energy absorbed during elastic deformation. Finally, the work hardening degree was also calculated as the difference between toughness and resilience.

Good 2nd-order correlations were found between σ_m and the amount of filler content and between work hardening and amount of filler content, Figure 10. However, the resilience is not influenced significantly by the MMT content, as shown Figure 11.

Results indicate that the filler content affects the deformation mechanisms during plastic deformation rather than the elastic deformation. At up to 2 wt % MMT content, the exfoliated particles interact strongly with polymeric chains, hindering plastic deformation and increasing the work hardening. According to Figure 6, in PU/MMT-5 that has contents of clay higher than 2%, part of the clay particles is agglomerated. Since the agglomerated clay (tactoids) should have lower interfacial contact area, it works as localized regions of stress concentration rather than as reinforcing agents.

Polymer swelling

All polymers obtained in this study absorb water when immersed in distilled water, as shown in Figure 13. The kinetics of water uptake differs for samples with and without nanoparticles. The rate of water uptake of PU/MMT-2 to PU/MMT-5 decreases with time going through a saturation limit, whereas PU/MMT-1 does not reach this limit (Fig. 12).

The obtained waterborne PU matrix and PU nanocomposites contain anionic hydrophilic groups and

TABLE II
Mechanical Properties of PU/MMT-1 to PU/MMT-5

PU	σ_m (MPa)	Resilience (MJ/m^3)	Toughness (MJ/m^3)	Work hardening (MJ/m^3)
PU/MMT-1	11.40 ± 0.14	2.09 ± 0.69	703.59 ± 10.62	701.50 ± 11.15
PU/MMT-2	19.81 ± 0.97	1.88 ± 0.14	1,053.49 ± 51.00	1,051.60 ± 51.11
PU/MMT-3	19.09 ± 1.98	1.50 ± 0.50	1,022.12 ± 99.19	1,020.61 ± 114.11
PU/MMT-4	23.75 ± 1.07	2.65 ± 0.04	1,300.42 ± 41.03	1,297.78 ± 40.99
PU/MMT-5	24.63 ± 2.49	1.40 ± 0.80	1,343.59 ± 167.45	1,342.18 ± 168.25

Obs.: σ_m = stress at 500% deformation.

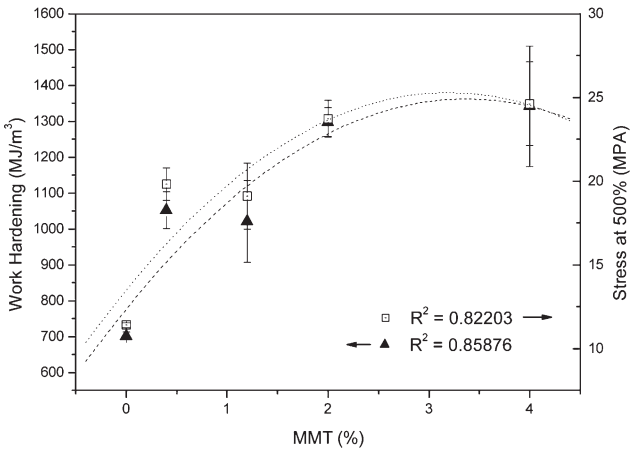

Figure 10 Influence of MMT content on σ_m and work hardening.

thus have high water affinity. As predicted by Figure 2, the nanocomposites have superior hydrophilicity (they have a larger number of surface polar groups and hydrophilic particles) and thus higher initial rates of water uptake. In the initial stage of water absorption, PU/MMT-4 showed the highest rate of water uptake due to the larger number of surface polar groups (Fig. 2) and higher degree of phase mixing [Fig. 5(b)] derived from the presence of better dispersed nanoparticles. For samples having higher concentrations of MMT than PU/MMT-4 (i.e., PU/MMT-5 that has 4 wt % of clay), the presence of agglomerates promotes the production of a PU having a lower degree of phase mixing and a less polar surface.

Alkaline degradation tests

The alkaline degradation tests aim to accelerate the hydrolytic degradation process of PU. Figure 13 shows the kinetics of alkaline degradation of the samples. The degradation process of some polyester

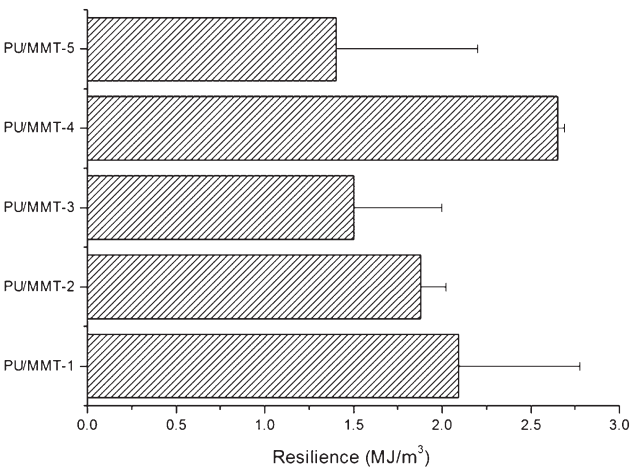

Figure 11 Influence of MMT content on resilience.

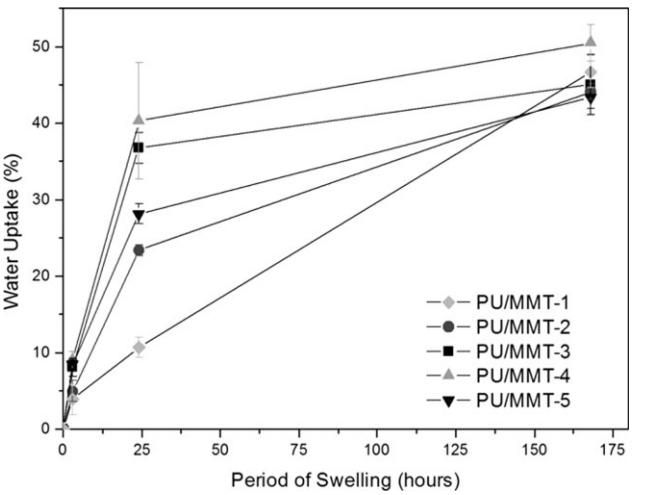

Figure 12 Water uptake of PU/MMT-1 to PU/MMT-5.

and PUs in alkaline solution is based on the hydrolytic attack of ester bonds.[21] As shown in Figure 13, this procedure caused a fast decay in sample mass during the first 4 h of the test. These results also show that clay particles enhance the rate of PU hydrolysis, mainly because the rate of water absorption in PUs containing clay is much higher than in pure PU within the first moments of the contact between water and the materials (as observed in Fig. 13).

Cellular viability

The cell viability measurements are presented in Figure 14 for cementoblasts cultured in contact with PU nanocomposites. There are no statistical differences in cell viability when PU nanocomposites are compared with the control. Therefore, PU nanocomposites can be considered nontoxic and capable of sustaining the proliferation of cementoblasts.

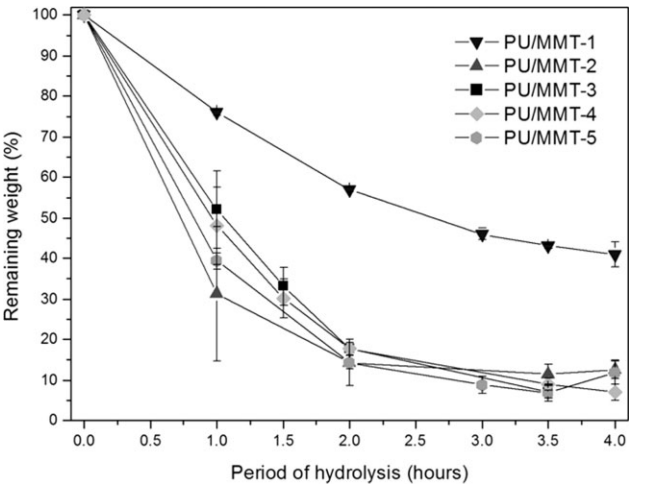

Figure 13 Alkaline degradation of PU/MMT-1 to PU/MMT-5.

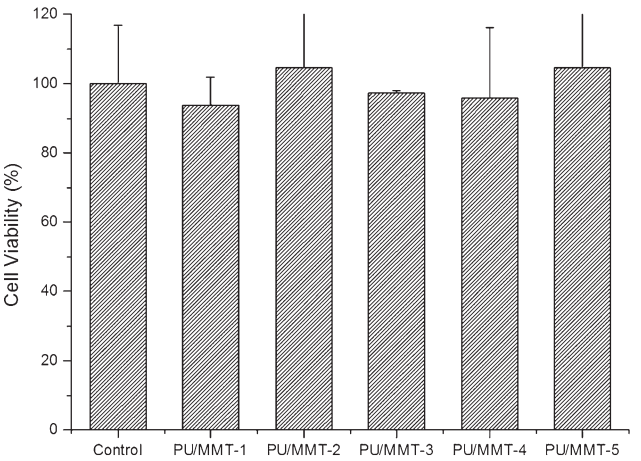

Figure 14 Results from the MTT assay for PU/MMT-1 to PU/MMT-5. The percentage of cell viability of all samples was calculated versus the control medium.

CONCLUSIONS

Exfoliated waterborne PU nanocomposites were successfully produced by direct solution blend. MMT content modified the degree of hydrogen bonding and the degree of phase separation, changing the matrix morphology. Data suggest that the incorporation of filler up to 2 wt % MMT resulted in highly well-dispersed and delaminated clay platelets that contributed to an enhancement in the degree of phase mixture of the system. PU nanocomposites containing clay particles in concentrations higher than 2 wt % MMT led to particle reagglomeration and phase separation. Both the rate of water absorption and the rate of hydrolytic degradation were increased by the presence of clay nanoparticles. Clay particles up 2 wt % were well dispersed in PU, leading to the formation of structures with higher degrees of phase mixing, polar surfaces, and displaying improvements in mechanical properties. The obtained PU nanocomposites provided a good environment for the adhesion and proliferation of cementoblasts. They can be considered suitable biomaterials for participating in procedures associated with periodontal regeneration.

The authors thank the National Synchrotron Light Laboratory (LNLS-Brazil) for the use of the SAXS beamline facilities.

References

1. Pan, H.; Chen, D. Eur Polym J 2007, 43, 3766.
2. Chen, G.; Ma, Y.; Zheng, X.; Xu, G. A.; Liu, J.; Fan, J.; Shen, D.; Qi, Z. J Polym Sci Part B: Polym Phys 2007, 45, 654.
3. Feng, Y. K.; Li, C. Y. Polym Degrad Stab 2006, 91, 1711.
4. Jeong, E. H.; Yang, J.; Lee, H. S.; Seo, S. W.; Baik, D. H.; Kim, J. J Appl Polym Sci 2008, 107, 803.
5. Wang, J.; Chen, Y.; Chen, R. J Polym Sci Part B: Polym Phys 2007, 45, 519.
6. Guelcher, S. A. Tissue Eng 2008, 14, 3.
7. Minnen, B. V.; Leeuwen, M. B. M. V. J Mater Sci Mater Med 2005, 16, 221.
8. Hou, L. T.; Yan, J. J.; Tsai, A. Y. M.; Lao, C. S.; Lin, S. J.; Liu, C. M. J. J Clin Periodontol 2004, 31, 68.
9. Takata, T.; Wang, H. L.; Miyauchi, M. J Periodontol Res 2001, 36, 322.
10. Warrer, K.; Karring, T.; Nyman, S.; Gogolewski, S. J Clin Periodontol 1992, 19, 633.
11. Coelho, M. B.; Pereira, M. M. J Biomed Mater B 2005, 75, 451.
12. Pereira, M. M.; Jones, J. R.; Oréfice, R. L.; Hench, L. L. J Mater Sci Mater Med 2005, 16, 1045.
13. Pereira, M. M.; Jones, R. L.; Hench, L. L. Adv Appl Ceram 2005, 104, 35.
14. Pereira, M. M.; Nazhat, S. N.; Jones, R. L.; Hench, L. L. Bioceramics 2005, 284, 757.
15. Valerio, P.; Guimaraes, M. H. R. J Mater Sci Mater Med 2005, 16, 851.
16. Valerio, P.; Pereira, M. M.; Goes, A. M.; Leite, M. F. Biomaterials 2004, 25, 2941.
17. Pereira, M. M.; Al-Saffar, N.; Selvakumaran, J.; Hench, L. L. Bioceramics 2005, 284, 589.
18. Kaneda, T.; Miyauchi, M.; Takekoshi, T.; Kitagawa, S.; Kitagawa, M.; Shiba, H.; Kurihara, H.; Takata, T. Bone 2004, 38, 420.
19. Chattopadhyay, D. K.; Sreedhar, B.; Raju, K. V. S. N. Polymer 2006, 47, 3814.
20. Bao, H.; Zhang, Z.; Ying, S. Polymer 1996, 37, 2751.
21. Ayres, E.; Oréfice, R. L.; Yoshida, M. I. Eur Polym J 2007, 43, 3510.
22. Marcos-Fernández, A.; Abraham, G. A.; Valentín, J. L.; San Román, J. Polymer 2006, 47, 785.
23. Gorna, K.; Gogolewski, S. Polym Degrad Stab 2002, 75, 113.
24. Gunes, I. S.; Jana, S. C. J Nanosci Nanotechnol 2008, 8, 1616.
25. Coates, J. P. Encyclopedia of Analytical Chemistry; Meyers, R. A., Ed.; Wiley: Chichester, UK, 2000; pp 10815–10837.
26. Jiang, X.; Li, J. H.; Ding, M. M.; Tan, H.; Ling, Q.; Zhong, Y.; Fu, Q. Eur Polym J 2007, 43, 1838.
27. Jia, Q. M.; Zheng, M.; Zhu, Y. C.; Li, J. B.; Xu, C. Z. Eur Polym J 2007, 43, 35.
28. Liu, Y.; Pan, C. Eur Polym J 1998, 34, 621.
29. Kim, B. H.; Choi, H. J.; Park, H. S.; Jeong, Y. D.; Jeong, H. D.; Lee, J. O.; Jo, N. J. Compos Interfaces 2006, 13, 285.
30. Tien, Y. I.; Wei, K. H. Polymer 2001, 42, 3213.
31. Wang, J. C.; Chen, Y. H.; Wang, J. L. J Appl Polym Sci 2006, 99, 3578.
32. Ayres, E. Poliuretanos e nanocompósitos biodegradáveis derivados de dispersões aquosas projetados para aplicações biomédicas; Tese Doutorado em Engenharia Metalúrgica e de Minad-Universidade Federal de Minas Gerais: Minas Gerais, 2006; 196 p.
33. Kim, B. K.; Lee, S. Y.; Xu, M. Polymer 1996, 37, 5781.
34. Xu, J.; Shi, W.; Pang, W. Polymer 2006, 47, 457.
35. Charnetskaya, A. G.; Polizos, G.; Shtompel, V. I.; Privalko, E. G.; Kercha, Y.; Pissis, P. Eur Polym J 2003, 39, 2167.
36. Wu, S.; Cheng, A.; Hua, H.; Shen, J. Polym Plast Technol Eng 2006, 45, 685.